NUCLEAR THEORY, Vol. 42 (2025)
eds. M. Gaidarov, N. Minkov, Heron Press, Sofia

Microscopic Study of Wobbling Motion Based on Relativistic Density Functional Theory

H.M. Dai, **Y.M. Wang**

East China Normal University, Shanghai 200241, China

Abstract.

Investigating wobbling motion provides crucial insights into the fundamental structure and excitation modes of nuclei, making it a frontier topic in both experimental and theoretical nuclear structure research. To search for the wobbling candidates in the realistic nuclei, a reliable theoretical approach is needed to get the information of the configuration and deformation for a specific nucleus. In this paper, the combination of relativistic density functional theory with particle rotor models or five-dimensional collective Hamiltonian approaches will be used to describe the wobbling candidates. We examine wobbling phenomena in the odd-mass isotope chains around $A \approx 160$, the $N = 59$ isotones in the $A \approx 100$ region, and the even-even nuclei. These studies reveal the possible existence of multiple wobbling modes in ^{167}Ta, transverse wobbling candidates in ^{97}Sr, ^{99}Zr, ^{101}Mo, ^{103}Ru, and ^{105}Pd, as well as even-even wobbler in ^{112}Ru.

1 Introduction

Wobbling motion is a distinctive rotational phenomenon in atomic nuclei with stable triaxial deformation [1]. In triaxially deformed nuclei, the moments of inertia differ along the three principal axes, favoring rotation about the axis with the largest moment of inertia to minimize rotational energy. However, coupling with rotations about the other axes can cause the nuclear rotation axis to deviate, resulting in wobbling motion [1]. When a triaxial rotor couples with a high-j valence particle, two types of wobbling modes emerge: longitudinal wobbling (LW), where the particle's or the total angular momentum aligns with the axis of the largest moment of inertia, and transverse wobbling (TW), where it is perpendicular [2, 3]. These modes correspond to the revolution of the total angular momentum around different principal axes, offering a unique probe of nuclear structure.

After the concept of wobbling motion was proposed, it was first experimentally confirmed to be ^{163}Lu in 2001 for the one-phonon wobbling excitation [4] and in 2002 for the two-phonon wobbling excitation [5]. The discovery of the wobbling nucleus ^{163}Lu has significantly stimulated interest in the search for other wobbling nuclei, with particular attention focused on nuclei in the $A \approx 160$ mass region. Wobbling motion has been identified in ^{161}Lu [6], ^{165}Lu [7],

^{167}Lu [8], and ^{167}Ta [9, 10]. These nuclei exhibit wobbling bands associated with the $\pi i_{13/2}$ configuration. Recently, ^{151}Eu [11] was identified as a wobbling nucleus with the $\pi h_{11/2}$ configuration. These experimental observations provide critical insights into the configuration structure and dynamical properties of triaxially deformed nuclei.

Beyond the $A \approx 160$ mass region, wobbling nuclei have also been observed in the $A \approx 100$, $A \approx 100$, and $A \approx 190$ mass regions. In the $A \approx 100$ and 130 regions, wobbling motion has been confirmed in ^{105}Pd [12], ^{135}Pr [13,14], ^{133}La [15], ^{130}Ba [16, 17], ^{125}Xe [18], ^{127}Xe [19], ^{133}Ba [20], and ^{136}Nd [21, 22]. Notably, ^{105}Pd is the only single-neutron wobbling nucleus identified in the $A \approx 100$ region. In the heavier region $A \approx 190$, ^{187}Au [23] and ^{183}Au [24] have been established as wobbling nuclei. Recently, in the light-mass region, ^{74}Br was proposed as the chiral wobbling nucleus with a $\pi g_{9/2} \otimes \nu g_{9/2}$ configuration [25].

The study of wobbling motion has attracted significant attention and has driven the rapid development of related theoretical work. Notable approaches include the random phase approximation (RPA) [26–35], the collective Hamiltonian method [36–39], and the angular momentum projection technique (or triaxial projected shell model) [21, 40–42]. The particle rotor model (PRM) is also widely used [2, 3, 17, 38, 43–55], along with its approximate solutions [56–63]. By coupling the rotational degrees of freedom of the nuclear core with the motion of valence particles, the PRM provides a systematic and quantitative approach to analyze wobbling phenomena.

The identification of wobbling nuclei within the nuclear chart requires a theoretical framework to elucidate their configuration and deformation characteristics. Relativistic density functional theory (RDFT), grounded in the mean-field approach, provides a powerful tool for this purpose. RDFT has been instrumental in delivering a fully microscopic and universal description of a wide range of nuclear phenomena [64–68]. Notably, the development of adiabatic and configuration-fixed constrained triaxial RDFT [69] has enabled detailed investigations into nuclear configurations and their associated deformations. This approach has been widely applied to explore the potential existence of nuclear wobbling [12, 17, 23, 24, 48, 50, 53, 54]. Hence, in this paper, the combination of RDFT with particle rotor model or five dimensional collective Hamiltonian approach will be used to describe the wobbling candidates.

2 Wobbling Motion with Single-Proton Configuration

The 160 nuclear region, as the first nuclear region discovered in wobbling motion, has been extensively studied. In these studies, wobbling bands were established on the $\pi i_{13/2}$ configuration. In this section, taking ^{167}Ta as an example, which is identified as a single-proton wobbling nucleus in the $\pi i_{13/2}$ configuration [9, 10]. We will explore the possible existence of the multiple wobbling bands in this nuclei. It is well known that high-j configurations and triaxial de-

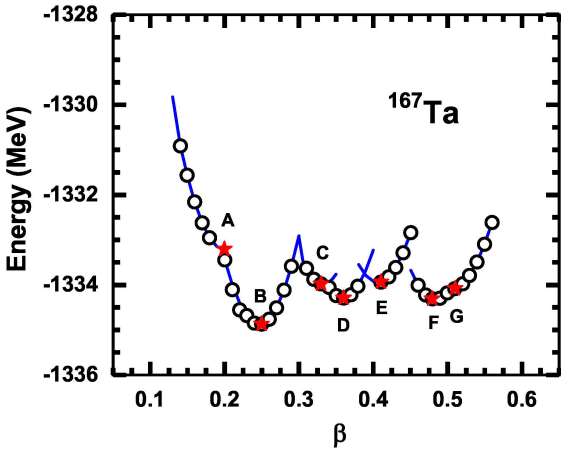

Figure 1. The potential energy curves as functions of deformation β in adiabatic (open circles) and configuration fixed (solid lines) constrained triaxial RDFT calculation for ^{167}Ta. The local minima in the energy surfaces for the fixed configuration are represented as stars and labeled as A, B, C, ... in accordance with the increasing β value. The shaded areas in the right panel of figure represent the triaxial deformation beneficial to the wobbling mode. Adapted from Ref. [54].

formation are necessary conditions for wobbling motion. Through RDFT, we can simultaneously obtain configuration and deformation information.

The potential energy curve results for ^{167}Ta, calculated using RDFT with PC-PK1 interaction [70], are presented in Figure 1. State A exhibits a local minimum with a valence nucleon configuration of $\pi(2d_{5/2})^{-1}(2d_{3/2})^{2}(1h_{11/2})^{-4}\otimes \nu(1h_{9/2})^{-2}(2f_{7/2})^{4}$, characterized by deformation parameters $\beta = 0.20$ and $\gamma = 0.0^{\circ}$. The unpaired nucleon configuration is $\pi(2d_{5/2})^{-1}$, corresponding to an axially symmetric, positive-parity, low-j particle configuration with the unpaired proton occupying the $d_{5/2}$ shell. The absence of significant triaxial deformation and high-j valence particle configurations precludes the formation of wobbling motion in this state. Similarly, state B, with a configuration of $\pi(2d_{3/2})^{1}(1h_{11/2})^{-4} \otimes \nu(1i_{13/2})^{2}(2f_{7/2})^{2}(1h_{9/2})^{6}$, $\beta = 0.25$, and $\gamma = 19.6^{\circ}$, features an unpaired nucleon configuration of $\pi(2d_{3/2})^{1}$. State D possesses a valence nucleon configuration of $\pi(2d_{5/2})^{-1}(1h_{9/2})^{2}(1h_{11/2})^{-4} \otimes \nu(1i_{13/2})^{4}(2f_{7/2})^{2}(1h_{9/2})^{4}$, with $\beta = 0.36$ and $\gamma = 22.6^{\circ}$. Its unpaired nucleon configuration, $\pi(2d_{5/2})^{-1}$, indicates a positive-parity, low-j orbital hole configuration with the unpaired proton at the apex of the $d_{5/2}$ shell. The valence nucleon configuration of state F also resides in low-j orbitals. None of these configurations are conducive to forming a wobbling band.

In contrast, state C in ^{167}Ta is characterized by a configuration of $\pi(1h_{9/2})^{1}$ $(1h_{11/2})^{-4} \otimes \nu(1i_{13/2})^{4}$ $(2f_{7/2})^{4}$ $(1h_{9/2})^{6}$, with deformation parameters $\beta = 0.33$ and $\gamma = 26.9^{\circ}$. The unpaired nucleon configuration, $\pi(1h_{9/2})^{1}$, cor-

responds to a negative-parity, high-j one-proton configuration exhibiting significant triaxial deformation, suggesting the potential for transverse wobbling (TW) motion. This differs from the currently observed wobbling bands in the $A \approx 160$ mass region, which are based on positive-parity $\pi(1i_{13/2})^1$ configurations. Thus, our theoretical findings provide a foundation for further experimental exploration of negative-parity wobbling bands. For state E, the local minimum configuration is $\pi(1h_{9/2})^3(1h_{11/2})^{-4}(2d_{5/2})^4 \otimes \nu(1i_{13/2})^4(1h_{9/2})^6$, with $\beta = 0.41$ and $\gamma = 18.7°$. The unpaired nucleon configuration, $\pi(1h_{9/2})^1$, mirrors that of state C but with the unpaired proton located in the middle of the shell, indicating a potential for longitudinal wobbling motion. Consequently, both states C and E exhibit characteristics conducive to wobbling motion.

The PRM facilitates the evaluation of the rotational properties of predicted nuclear configurations and their potential to exhibit wobbling modes. With the obtained deformation parameters from the RDFT calculations, the PRM calculations were carried out to study the spectroscopic properties [54].

The energy difference $\Delta E(I)$ between the doublet bands is an essential criterion for judging the type of wobbling motion. The decreased and increased $\Delta E(I)$ indicate, respectively, a TW and LW [2]. The energy difference between

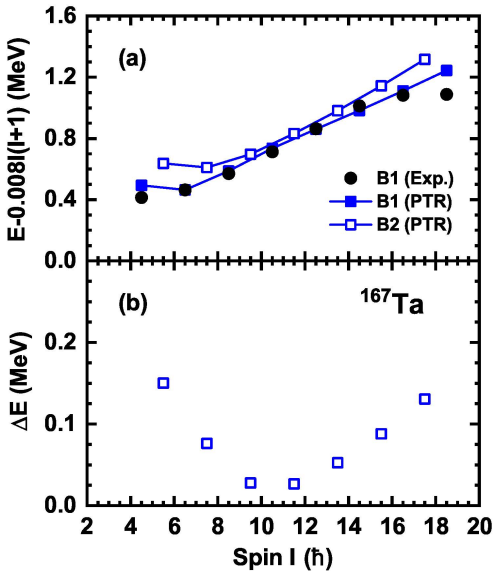

Figure 2. The lowest bands B1 and B2 built on the configuration $\pi(1h_{9/2})^1$ in ^{167}Ta. (a) The calculated energy spectra minus a common rigid rotor reference in comparison with the available experimental data in Ref. [10]. (b) Theoretical energy difference between the doublet bands B1 and B2. Adapted from Ref. [54].

bands B1 and B2 is calculated as

$$\Delta E(I) = E_{\mathrm{B2}}(I) - \frac{1}{2}\Big[E_{\mathrm{B1}}(I+1) + E_{\mathrm{B1}}(I-1)\Big]. \quad (1)$$

The PRM calculations well reproduce the experimental data with signature $\alpha = +1/2$, as shown in Figure 2(a). Its signature partner band (called as bands B2) with $\alpha = -1/2$ is also obtained simultaneously. Using Eq. (1), we calculate $\Delta E(I)$ and display it in Figure 2(b), which exhibits a trend of decreasing initially and then increasing, indicating a transition from TW to LW [2, 3]. The critical spin occurs at $I = 23/2\hbar$. This implies the possibility of multiple wobbling modes in ^{167}Ta based on the previously observed $i_{13/2}$ configuration [9,10] and currently studied $h_{9/2}$ configuration.

3 Wobbling motion with single-neutron configuration

In the mass region of $A \approx 100$, the nucleus ^{105}Pd, with an odd neutron number $N = 59$, is a promising candidate for exhibiting wobbling motion. It has been identified as a TW candidate, with its first wobbling excited state based on single-neutron configuration [12]. Consequently, investigating the potential existence of wobbling nuclei in this mass region, particularly within the $N = 59$ isotone chain, is of significant scientific interest.

In this section, we employ constrained RDFT calculations to investigate the configurations and triaxial deformations of $N = 59$ isotones [50] in the $A \approx 100$ mass region, specifically ^{95}Kr ($Z = 36$), ^{97}Sr ($Z = 38$), ^{99}Zr ($Z = 40$), ^{101}Mo ($Z = 42$), ^{103}Ru ($Z = 44$), ^{105}Pd ($Z = 46$), and ^{107}Cd ($Z = 48$), to explore the possible presence of wobbling modes.

To investigate the wobbling modes, the PECs as a function of the deformation parameter β are calculated for ^{95}Kr, ^{97}Sr, ^{99}Zr, ^{101}Mo, ^{103}Ru, ^{105}Pd, and ^{107}Cd using adiabatic RDFT calculations. The results are presented in Figure 3. In these calculations, constraints are applied to $\langle \hat{Q}_{20}^2 + 2\hat{Q}_{22}^2 \rangle$, equivalent to β^2, with triaxial deformations determined automatically through energy minimization. In Figure 3, open circles denote the outcomes of adiabatic calculations, which produce irregular energy curves, with some local minima being too indistinct to identify clearly. Configuration-fixed calculations effectively resolve this issue [69], and their results are depicted as lines in Figure 3. The minima in each curve are marked by red stars and labeled with capital letters A, B, C, ..., in order of increasing β values. The ground-state deformation parameters derived from these configuration-fixed calculations correspond to local minima B for ^{95}Kr, G for ^{97}Sr, E for ^{99}Zr, G for ^{101}Mo, C for ^{103}Ru, A for ^{105}Pd, and A for ^{107}Cd. To sum up, only the nucleus ^{103}Ru has significant triaxial deformation and a high-j particle configuration among these nuclei. Therefore, the ground state of ^{103}Ru satisfies the both conditions for the wobbling mode.

In addition to the ground state, some excited states might also have the wobbling modes. It is interesting to note that the excited states of other nuclei also

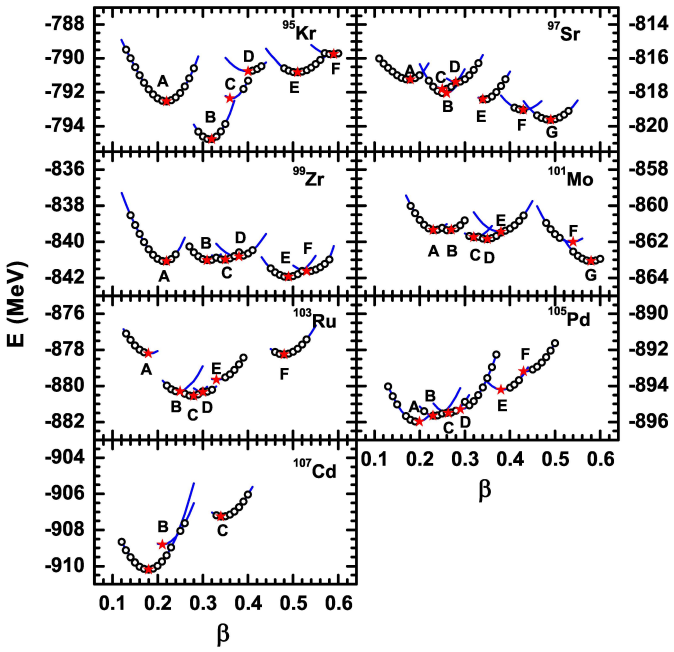

Figure 3. The potential energy curves as functions of deformation β in adiabatic (open circles) and configuration fixed (solid lines) constrained triaxial RDFT calculation for ^{95}Kr, ^{97}Sr, ^{99}Zr, ^{101}Mo, ^{103}Ru, ^{105}Pd, and ^{107}Cd. The local minima in the energy surfaces for the fixed configuration are represented as stars and labeled as A, B, C, ... in accordance with the increasing β value. The shaded areas in the right panel of figure represent the triaxial deformation beneficial to the wobbling mode. Adapted from Ref. [50].

have significant triaxial deformation, which indicate that they might have wobbling modes as well. The states are as follows: A (β = 0.22, γ = 35.9°) in ^{95}Kr, C (β = 0.25, γ = 37.9°), and D (β = 0.28, γ = 30.0°) in ^{97}Sr, B (β = 0.31, γ = 23.3°) in ^{99}Zr, A (β = 0.23, γ = 25.9°), B (β = 0.27, γ = 22.9°), and C (β = 0.32, γ = 21.6°) in ^{101}Mo, B (β = 0.25, γ = 20.4°) in ^{103}Ru, as well as B (β = 0.23, γ = 22.2°), C (β = 0.27, γ = 24.9°), and D (β = 0.29, γ = 30.7°) in ^{105}Pd. One notes that the wobbling bands originated from the state C in ^{105}Pd has been reported experimentally [12].

To present the detailed results of the configuration-fixed constrained RDFT calculations, the energies, deformation parameters β and γ, valence nucleon configurations, and unpaired nucleon configurations for the local minima in ^{95}Kr, ^{97}Sr, ^{99}Zr, ^{101}Mo, ^{103}Ru, and ^{105}Pd are compiled in Table 1. The table shows the information of states with significant triaxial deformation. Analysis of the table reveals that the following states exhibit both significant triaxial deformation and high-j particle conditions: state D ($\beta = 0.28$, $\gamma = 30.0°$) in ^{97}Sr, state B ($\beta = 0.31$, $\gamma = 23.3°$) in ^{99}Zr, states B ($\beta = 0.27$, $\gamma = 22.9°$) and

Table 1. The configurations (both valence and unpaired nucleon) as well as the corresponding energies (in MeV) and the deformation parameters β and γ (in degree) for the local minima in ^{95}Kr, ^{97}Sr, ^{99}Zr, ^{101}Mo, ^{103}Ru and ^{105}Pd obtained by the configuration fixed constrained triaxial RDFT calculations.

Nucleus	State	Valence-cfg.	Unpaired-cfg.	Energy	β	γ
^{95}Kr	A	$\pi(2p_{3/2})^2 \otimes \nu[(1g_{7/2})^4(2d_{3/2})^1]$	$\nu(2d_{3/2})^1$	−792.53	0.22	35.9°
^{97}Sr	C	$\pi[(1g_{9/2})^2(2p_{3/2})^2] \otimes \nu[(2d_{3/2})^{-1}(1g_{7/2})^{-2}]$	$\nu(2d_{3/2})^1$	−817.80	0.25	37.9°
	D	$\pi[(2p_{3/2})^2(1g_{9/2})^2] \otimes \nu[(1h_{11/2})^1(1g_{7/2})^{-2}]$	$\nu(1h_{11/2})^1$	−817.40	0.28	30.4°
^{99}Zr	B	$\pi(1g_{9/2})^4 \otimes \nu(1h_{11/2})^1$	$\nu(1h_{11/2})^1$	−841.02	0.31	23.3°
^{101}Mo	A	$\pi(1g_{9/2})^4 \otimes \nu[(1g_{7/2})^{-3}(2d_{5/2})^{-2}]$	$\nu(1g_{7/2})^1$	−861.34	0.23	25.9°
	B	$\pi[(2p_{3/2})(1g_{9/2})^4] \otimes \nu[(1h_{11/2})^1(1g_{7/2})^6]$	$\nu(1h_{11/2})^1$	−861.34	0.27	22.9°
	C	$\pi(1g_{9/2})^6 \otimes \nu[(1h_{11/2})^1(1g_{7/2})^6]$	$\nu(1h_{11/2})^1$	−861.74	0.32	21.6°
^{103}Ru	B	$\pi(1g_{9/2})^6 \otimes \nu[(1g_{7/2})^{-3}(2d_{5/2})^2]$	$\nu(1g_{7/2})^1$	−880.30	0.25	20.4°
	C	$\pi(1g_{9/2})^6 \otimes \nu[(1h_{11/2})^1(2d_{5/2})^2]$	$\nu(1h_{11/2})^1$	−880.55	0.28	21.3°
^{105}Pd	B	$\pi(1g_{9/2})^{-2} \otimes \nu[(1g_{7/2})^5(2d_{5/2})^4]$	$\nu(1g_{7/2})^1$	−895.65	0.23	22.2°
	C	$\pi(1g_{9/2})^{-2} \otimes \nu[(1h_{11/2})^1(1g_{7/2})^6(2d_{3/2})^2]$	$\nu(1h_{11/2})^1$	−895.49	0.27	24.9°
	D	$\pi(1g_{9/2})^{-2} \otimes \nu[(1g_{7/2})^5(2d_{3/2})^2(1h_{11/2})^2]$	$\nu(1g_{7/2})^1$	−895.29	0.29	30.7°

C ($\beta = 0.32$, $\gamma = 21.6°$) in ^{101}Mo, and state C ($\beta = 0.26$, $\gamma = 24.9°$) in ^{105}Pd. Consequently, the excited states in ^{97}Sr, ^{99}Zr, ^{101}Mo, and ^{105}Pd are conducive to forming wobbling modes, with their unpaired nucleon configurations all based on $\nu(1h_{11/2})^1$. Notably, ^{101}Mo exhibits two configurations suitable for wobbling modes, suggesting the potential for multiple wobbling modes.

4 Wobbling motion in even-even nuclei

The wobbling motion was initially predicted in even-even nuclei without the valence quasi-particles, but the experimental evidence for this is still rare [16]. In order to inspect the existence of wobbling motion, the spin coherent state (SCS) probability density distribution $\mathcal{P}(\theta, \varphi)$ (or called as the azimuthal plot [45, 71]) for the orientation of the total angular momentum $\boldsymbol{J}$ on the $\theta\varphi$-sphere is incorporated to the five dimensional collective Hamiltonian [39, 72–75] framework and and shown in Figure 4 for states in the ground-state band and γ-band for ^{112}Ru. Here, θ is a polar angle between the total angular momentum $\boldsymbol{J}$ and the long (l) axis, and φ is an azimuthal angle in the short-intermediate (sm) plane measured from the intermediate (m) axis.

For states in the ground-state band of ^{112}Ru, the probability distribution $\mathcal{P}(\theta, \varphi)$ exhibits a maximum at $\varphi = 0°$, indicating the highest likelihood of aligning the total angular momentum $\boldsymbol{J}$ along the m axis. In contrast, states in the γ-band display a minimum at $\varphi = 0°$, manifesting as a node along the m axis due to wobbling excitation relative to this axis. For these γ-band states, the maximum probability forms a rim encircling the minimum, with $\mathcal{P}(\theta, \varphi)$ reflecting the characteristic wobbling motion of $\boldsymbol{J}$ about the m axis. This distribution aligns with the expected pattern for wobbling motion in such nuclear configurations.

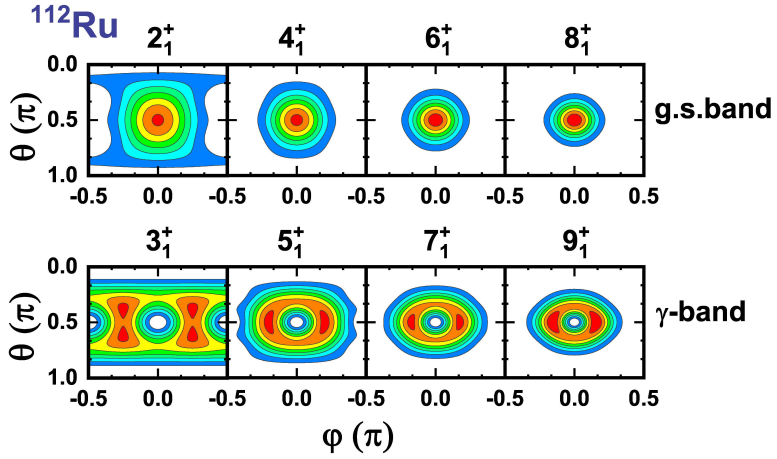

Figure 4. The SCS probability densities $\mathcal{P}(\theta, \varphi)$ calculated by 5DCH for states in the ground-state band and γ-band of ^{112}Ru. Adapted from Ref. [39].

5 Summary

In summary, we examine wobbling phenomena in the odd-mass isotope chains around $A \approx 160$, the $N = 59$ isotones in the $A \approx 100$ region, and even-even nuclei. These studies reveal the possible existence of multiple wobbling modes in ^{167}Ta, transverse wobbling candidates in ^{97}Sr, ^{99}Zr, ^{101}Mo, ^{103}Ru, and ^{105}Pd, as well as even-even wobbler in ^{112}Ru.

Acknowledgements

The authors would like to thank Qibo Chen for his suggestions and reading the manuscript, and acknowledge Xianrong Zhou and Yu Shu for their contributions to this work. This work was supported by the National Natural Science Foundation of China under Grants No. 12575123 and No. 12205103, and the National Key R&D Program of China No. 2024YFE0109803.

References

[1] A. Bohr, B.R. Mottelson, *Nuclear structure* (Benjamin, New York, 1975).

[2] S. Frauendorf, F. Dnau, *Phys. Rev. C* **89** (2014) 014322.

[3] Q.B. Chen, S. Frauendorf, *Eur. Phys. J. A* **58** (2022) 75.

[4] S.W. Ødegård, G.B. Hagemann, D.R. Jensen *et al.*, *Phys. Rev. Lett.* **86** (2001) 5866.

[5] D.R. Jensen, G.B. Hagemann, I. Hamamoto *et al.*, *Phys. Rev. Lett.* **89** (2002) 142503.

[6] P. Bringel, G.B. Hagemann, H. Hübel *et al.*, *Eur. Phys. J. A* **24** (2005) 167.

[7] G. Schönwaßer, H. Hübel, G.B. Hagemann *et al.*, *Phys. Lett. B* **552** (2003) 9.
[8] H. Amro, W.C. Ma, G.B. Hagemann *et al.*, *Phys. Lett. B* **553** (2003) 197.
[9] D.J. Hartley, R.V.F. Janssens, L.L. Riedinger *et al.*, *Phys. Rev. C* **80** (2009) 041304.
[10] D.J. Hartley, R.V.F. Janssens, L.L. Riedinger *et al.*, *Phys. Rev. C* **83** (2011) 064307.
[11] A. Mukherjee, S. Bhattacharya, T. Trivedi *et al.*, *Phys. Rev. C* **107** (2023) 054310.
[12] J. Timár, Q.B. Chen, B. Kruzsicz *et al.*, *Phys. Rev. Lett.* **122** (2019) 062501.
[13] J.T. Matta, U. Garg, W. Li *et al.*, *Phys. Rev. Lett.* **114** (2015) 082501.
[14] N. Sensharma, U. Garg, S. Zhu *et al.*, *Phys. Lett. B* **792** (2019) 170.
[15] S. Biswas, R. Palit, S. Frauendorf *et al.*, *Eur. Phys. J. A* **55** (2019) 159.
[16] C.M. Petrache, P.M. Walker, S. Guo *et al.*, *Phys. Lett. B* **795** (2019) 241.
[17] Q.B. Chen, S. Frauendorf, C.M. Petrache, *Phys. Rev. C* **100** (2019) 061301.
[18] M. Prajapati, S. Nag, A.K. Singh *et al.*, *Phys. Rev. C* **109** (2024) 034301.
[19] S. Chakraborty, H. Sharma, S. Tiwary *et al.*, *Phys. Lett. B* **811** (2020) 135854.
[20] K. Rojeeta Devi, S. Kumar, N. Kumar *et al.*, *Phys. Lett. B* **823** (2021) 136756.
[21] F.Q. Chen, C.M. Petrache, *Phys. Rev. C* **103** (2021) 064319.
[22] B.F. Lv, C.M. Petrache, R. Budaca *et al.*, *Phys. Rev. C* **105** (2022)034302.
[23] N. Sensharma, U. Garg, Q.B. Chen *et al.*, *Phys. Rev. Lett.* **124** (2020) 052501.
[24] S. Nandi, G. Mukherjee, Q.B. Chen *et al.*, *Phys. Rev. Lett.* **125** (2020) 132501.
[25] R.J. Guo, S.Y. Wang, C. Liu *et al.*, *Phys. Rev. Lett.* **132** (2024) 092501.
[26] E.R. Marshalek, *Nucl. Phys. A* **275** (1977) 416.
[27] Y. R. Shimizu and M. Matsuzaki,*Nucl. Phys. A*, **588**, (1995) 559.
[28] M. Matsuzaki, Y.R. Shimizu, K. Matsuyanagi, *Phys. Rev. C* **65** (2002) 041303.
[29] M. Matsuzaki, Y.R. Shimizu, K. Matsuyanagi, *Eur. Phys. J. A* **20** (2003) 189.
[30] M. Matsuzaki, Y.R. Shimizu, K. Matsuyanagi, *Phys. Rev. C* **69** (2004) 034325.
[31] Y.R. Shimizu, M. Matsuzaki, K. Matsuyanagi, *Phys. Rev. C* **72** (2005) 014306.
[32] D. Almehed, R.G. Nazmitdinov, F. Doenau, *Phys. Scr.* **T125** (2006) 139.
[33] Y.R. Shimizu, T. Shoji, M. Matsuzaki, *Phys. Rev. C* **77** (2008) 024319.
[34] T. Shoji, Y.R. Shimizu, *Progr. Theor. Phys.* **121** (2009) 319.
[35] S. Frauendorf, F. Dönau, *Phys. Rev. C* **92** (2015) 064306.
[36] Q.B. Chen, S.Q. Zhang, P.W. Zhao, J. Meng, *Phys. Rev. C* **90** (2014) 044306.
[37] Q.B. Chen, S.Q. Zhang, J. Meng, *Phys. Rev. C* **94** (2016) 054308.
[38] Q.B. Chen, S. Frauendorf, *Phys. Rev. C* **109** (2024) 044304.
[39] Y.M. Wang, Q. B. Chen, *Phys. Lett. B* **859** (2024) 139131.
[40] M. Shimada, Y. Fujioka, S. Tagami, Y.R. Shimizu, *Phys. Rev. C* **97** (2018) 024318.
[41] Y.K. Wang, F.Q. Chen, P.W. Zhao, *Phys. Lett. B* **802** (2020) 135246.
[42] S.A. Bhat, S. Jehangir, G.H. Bhat, J.A. Sheikh, G.B. Vakil, *Phys. Rev. C* **111** (2025) 054310.
[43] I. Hamamoto, *Phys. Rev. C* **65** (2002) 044305.
[44] I. Hamamoto, G.B. Hagemann, *Phys. Rev. C* **67** (2003) 014319.
[45] E. Streck, Q.B. Chen, N. Kaiser, U.-G. Meißner, *Phys. Rev. C* **98** (2018) 044314.
[46] Q.B. Chen, S. Frauendorf, N. Kaiser, U.-G. Meißner, J. Meng, *Phys. Lett. B* **807** (2020) 135596.
[47] C. Broocks, Q.B. Chen, N. Kaiser, U.-G. Meißner, *Eur. Phys. J. A* **57** (2021) 161.

[48] L. Hu, J. Peng, Q.B. Chen, *Phys. Rev. C* **104** (2021) 064325.
[49] H. Zhang, B. Qi, X.D. Wang, H. Jia, S.Y. Wang, *Phys. Rev. C* **105** (2022) 034339.
[50] H.M. Dai, Q.B. Chen, X.-R. Zhou, *Phys. Rev. C* **108** (2023) 054306.
[51] S. H. Li, H.M. Dai, Q.B. Chen, X.-R. Zhou, *Chin. Phys. C* **48** (2024) 034102.
[52] H.M. Dai, Q.B. Chen, *Phys. Rev. C* **109** (2024) 054321.
[53] Y.Z. Ji, Q.B. Chen, *Phys. Rev. C* **111** (2025) 034328.
[54] H.M. Dai, Y. Shu, Q.B. Chen, *Phys. Rev. C* **111** (2025) 054313.
[55] H. Jia, M.Q. Zhou, L. Mu, H. Zhang, L. Liu, B. Qi, *Eur. Phys. J. A* **60** (2024) 240.
[56] A.A. Raduta, R. Poenaru, L.G. Ixaru, *Phys. Rev. C* **96** (2017) 054320.
[57] K. Tanabe, K. Sugawara-Tanabe, *Phys. Rev. C* **95** (2017) 064315.
[58] A.A. Raduta, R. Poenaru, A.H. Raduta, *J. Phys. G: Nucl. Part. Phys.* **45** (2018) 105104.
[59] R. Budaca, *Phys. Rev. C* **97** (2018) 024302.
[60] E.A. Lawrie, O. Shirinda, C.M. Petrache, *Phys. Rev. C* **101** (2020) 034306.
[61] R. Budaca, *Phys. Rev. C* **103** (2021) 044312.
[62] R. Budaca, C.M. Petrache, *Phys. Rev. C* **106** (2022) 014313.
[63] Yeruoxi Chen, Q.B. Chen, R.V. Jolos, *Phys. Rev. C* **111** (2025) 064313.
[64] P.G. Reinhard, *Rep. Prog. Phys.* **52** (1989) 439.
[65] P. Ring, *Prog. Part. Nucl. Phys.* **37** (1996) 193.
[66] D. Vretenar, A. Afanasjev, G. Lalazissis, P. Ring, *Phys. Rep.* **409** (2005) 101.
[67] J. Meng, H. Toki, S.-G. Zhou, S.Q. Zhang, W.H. Long, L.S. Geng, *Prog. Part. Nucl. Phys.* **57** (2006) 470.
[68] J. Meng, Ed., *Relativistic density functional for nuclear structure, ser. International Review of Nuclear Physics* (Singapore: World Scientific 2016) **10**.
[69] J. Meng, J. Peng, S.Q. Zhang, S.-G. Zhou, *Phys. Rev. C* **73** (2006) 037303.
[70] P.W. Zhao, Z.P. Li, J.M. Yao, J. Meng, *Phys. Rev. C* **82** (2010) 054319.
[71] F.Q. Chen, Q.B. Chen, Y.A. Luo, J. Meng, S.Q. Zhang, *Phys. Rev. C* **96** (2017) 051303.
[72] T. Nikšić, Z.P. Li, D. Vretenar, L. Próchniak, J. Meng, P. Ring, *Phys. Rev. C* **79** (2009) 034303.
[73] Z.P. Li, T. Nikšić, D. Vretenar, J. Meng, G.A. Lalazissis, P. Ring, *Phys. Rev. C* **79** (2009) 054301.
[74] T. Nikšić, D. Vretenar, P. Ring, *Prog. Part. Nucl. Phys.* **66** (2011) 519.
[75] Z.P. Li, T. Nikšić, D. Vretenar, *J. Phys. G: Nucl. Part. Phys.* **43** (2016) 024005.